Aerospace Sciences Meeting, 10-13 January 2005, Reno, NV

A Tank Self-Pressurization Experiment Using a Model Fluid in Normal Gravity

Stephen Barsi*
Case Western Reserve University

Mohammad Kassemi†
National Center for Microgravity Research

Charles H. Panzarella‡
Ohio Aerospace Institute

J. Iwan D. Alexander§
Case Western Reserve University

The self-pressurization rate of a cryogenic storage tank has important design consequences for propellant and life support systems currently being planned for long duration space missions. The amount of liquid in the tank and the heat leak rate and distribution can all have an effect on the pressurization rate. To investigate these effects, a model fluid experiment is undertaken in normal gravity. Experimental results show, after undergoing an initial transience, the tank pressure increases at a uniform rate. Moreover, the data reveals that the thermal inertia of the tank wall cannot be neglected in the present study. Consequently, a thermodynamic model that includes these wall effects is developed. Comparisons show excellent agreement between the pressurization rate predicted by the thermodynamic model and the empirically obtained pressurization rate when the heat is added to the liquid, but discrepancies arise when heat is added directly to the vapor. The thermodynamic model also fails to capture the initial pressure behavior of the system as well as the effect of heat distribtuion on the pressurization rate. To resolve these shortcomings, more sophisticated computational models are required.

Nomenclature

c	Specific heat capacity, J/kg K
e	Specific internal energy, J/kg
k	Thermal conductivity, W/m K
L	Latent heat, J/kg
p	Pressure, Pa
$\dot{Q}$	Heater power, W
R	Gas constant, J/kg K
T	Temperature, K
t	Time, s
V	Volume, m^3
ρ	Density, kg/m^3

Subscript

l	Liquid
T	Tank
v	Vapor
w	Wall

*AIAA Student Member
†21000 Brookpark Rd., MS:110-3, Cleveland, OH 44135,AIAA Member.
‡AIAA Member
§AIAA Member

I. Introduction

Since the early days of the space program, cryogenic fluid management has had important implications for propellant systems and for life support systems.[1] Any heat leak into a cryogenic storage tank either through solar radiation, aerodynamic heating or conduction loads from the tank support structure can lead to a significant rise in tank pressure. Heat entering from the tank walls will be carried to the liquid vapor interface by convection currents generated by density gradients in the liquid. As the warmer fluid reaches the interface, evaporation will occur resulting in ullage compression and a subsequent rise in tank pressure.

A significant increase in ullage pressure can lead to structural failure of the storage tank and/or a decrease in the net positive suction head at an engine inlet. Both possibilities increase the risk of a catastrophic mission failure.

While a number of technologies have been developed[2] or proposed[3] to combat the undesirable effects of tank self-pressurization, a more fundamental investigation of the actual process has been the subject of numerous experimental, analytical, and computational studies.

Aydelott investigated tank self-pressurization in a small-scale partially filled liquid hydrogen container in both low gravity and normal gravity.[4] He showed that tank geometry and size, heat transfer rate and distribution, liquid fill fraction and gravity level all affect the rate of pressure rise in a closed cryogenic container. Liebenberg and Edeskuty experimentally studied pressurization in a large scale liquid hydrogen dewar.[5] Unfortunately, their pressure measurements did not agree well with their simple analytical model. The pressurization rate was underpredicted by a factor of ten. They suggested the discrepancy was due to the thermal stratification that existed in the bulk liquid at the liquid-vapor interface.

To better understand this pressurization behavior, Aydelott and Spuckler investigated how the pressurization rate scales with tank size for a uniformly distributed heat flux.[6] They suggested that the pressure rise rate can be expressed as a function of volumetric heating. Indeed, such a term appears in the the thermodynamic model of Riemer[7] and Lin *et al.*[8] Unfortunately application of similar homogeneous thermodynamic models to experimental data has resulted in deviations with the measured pressurization rate.[4]

To resolve these discrepancies more sophisticated computational models have been developed. One approach has been to numerically integrate the conservation equations across a natural convection boundary layer along the side wall of the tank.[9] This formulation presumes a well defined natural convection boundary layer exists on the side wall. However, analysis from liquid hydrogen rocket propellant tanks suggests otherwise.[10] Instead of only analyzing the thermal boundary layer on the side wall, another approach has been to study the stratification problem by solving the transport equations in the liquid.[11,12,13] To the simplify the analysis, vapor pressurization, is typically neglected. Recently, attempts have been made to couple the transport processes in the liquid with a lumped thermodynamic model of the vapor.[14] The results of the lumped-vapor active-liquid model have been compared to homogeneous thermodynamic models and in all cases comparisons showed excellent agreement between the self-pressurization rate predicted by the numerical simulation to that predicted by the thermodynamic model. To validate this and other models, in the present study, a self-pressurization experiment using a model fluid is conducted in normal gravity. Specifically, the effects of heat input, liquid fill fraction, and heat distribution are investigated. Relevant trends will be discussed and comparisons will be made to a homogeneous thermodynamic model.

II. Experimental Apparatus and Procedures

A schematic of the model fluid experiment is shown in Fig. 1. The model fluid is HFE-7000 (3M), a refrigerant-like fluid with a low normal boiling point (34 °C). Initially all the fluid is contained in the reservoir tank. To purge dissolved gas impurities from the fluid, a vacuum pump lowers the pressure in the reservoir. As the partial pressures of the dissolved gases are reduced, the contaminant species will come out of solution. The contaminants along with some HFE vapor pass through a liquid nitrogen cold trap before being vented outside. Any HFE condensate in the cold trap is reclaimed for later use. Once the desired purity levels are achieved, the test cell is evacuated before undergoing a no-vent fill process. Fluid is pumped from the reservoir to the test cell until the desired fill fraction is reached. Since venting does not occur during the fill process, ullage compression takes place as liquid is being pumped into the test cell. Thus, when the specified fill fraction is reached, the vapor and liquid are not in equilibrium. Eventually the liquid and vapor will equilibrate. To accelerate the equilibration process, fluid is withdrawn from the test cell and

pumped through a heat exchanger before entering the tank through an axial jet. The second fluid in the heat exchanger is distilled water, whose temperature and flow rate are controlled by a temperature-controlled recirculating bath. The temperature of HFE is monitored downstream of the pump and heat exchanger. The bath monitors this temperature and adjusts the temperature of the distilled water accordingly so that the desired set point temperature of HFE is maintained. This equilibration process continues for approximately four hours prior to the experiment until the ullage pressure becomes time invariant.

The test cell consists of a cylindrical acrylic body 16" x 8" x 1" (length x inner diameter x wall thickness) with curved acrylic end caps (radius of curvature = 8.5"). The total tank volume is 855.55 in^3.

To simulate heat leak from the environment, two 1" wide kapton foil strip heaters are mounted to the inside surface of the test cell. The heaters are mounted to the inner wall using a combination of pressure sensitive adhesive and flat copper springs (1/16" in width). To record the pressure in the ullage, a pressure transducer ($\pm$0.01 psi) is mounted to the top of the test cell. To record point measurements of temperature inside the test cell, fourteen thermistors enter the tank through the side wall and one thermistor enters the tank from the top cap. The accuracy of the thermistors is $\pm$0.01 °C. Additional temperature measurements include ten RTD elements ($\pm$0.1 °C) that are cemented to the outer wall of the test cell and a thermistor measurement ($\pm$0.1 °C) of the ambient laboratory temperature around the test cell. All transducer measurements are sent to a data recorder and then saved to a laptop in real time at 1 Hz.

Before the experiment is about to begin, the equilbration process ends: the recirculation jet is turned off and the valves separating the test cell from the recirculation loop are closed. The resistance of the heating strips are measured and the voltage source meters for the heaters are programmed to achieve the desired heat leak rate. The source meters are extremely stable with a maximum variation in heater power of 0.01% throughout the duration of the experiment. At time = 0, power is supplied to the heating strips and the tank is allowed to self-pressurize. At the end of the experiment, fluid is transferred back into the reservoir tank.

III. Mathematical Model

Several assumptions are invoked in order to derive this thermodynamic model. The primary assumption is that the fluid and vapor are at the same temperature and pressure and that temperature and pressure are related through a saturation condition. Secondary assumptions are that the tank wall is in thermal equilibrium with the fluid and vapor, the fluid is incompressible, and the thermal properties of the liquid and vapor are constant.

Using these assumptions, for a rigid tank, the first law of thermodynamics becomes:

$$\frac{d}{dt}\left(\rho_v V_v e_v + \rho_l V_l e_l + \rho_w V_w e_w\right) = \dot{Q} \tag{1}$$

where ρ is the density, V is the volume, e is the internal energy, $\dot{Q}$ is the heat leak rate, and the subscripts v, l, and w denote the vapor, liquid, and wall regions of the system. Space conservation requires that:

$$V_l = V_T - V_v \tag{2}$$

where V_T is the volume within the tank. Since the tank is a closed system, mass conservation requires that:

$$\frac{d}{dt}(\rho_v V_v) + \frac{d}{dt}(\rho_l V_l) = 0 \tag{3}$$

Substituing Equation (2) into Equation (1) and expanding yields:

$$\dot{\rho_v} V_v e_v + \rho_v \dot{V_v} e_v + \rho_v V_v \dot{e_v} + \rho_l V_l \dot{e_l} - \rho_l \dot{V_v} e_l + \rho_w V_w \dot{e_w} = \dot{Q} \tag{4}$$

The internal energy can be computed from an arbitrary reference state assuming constant specific heat:

$$e = c(T - T_o) + e_o \tag{5}$$

The time derivative of the internal energy is thus:

$$\dot{e} = c\dot{T} \tag{6}$$

Equation (4) can now be rewritten:

$$\left[\rho_v V_v c_v + \rho_l V_l c_l + \rho_w V_w c_w\right] \frac{dT}{dt} + \frac{d(\rho_v V_v)}{dt} e_v - \rho_l \frac{dV}{dt} e_l = \dot{Q} \tag{7}$$

But from mass conservation:

$$\rho_l \frac{dV_v}{dt} = -\frac{d}{dt}\Big(\rho_l (V_T - V_v)\Big) = \frac{d(\rho_v V_v)}{dt} \tag{8}$$

Thus, Equation (7) becomes:

$$\left[\rho_v V_v c_v + \rho_l V_l c_l + \rho_w V_w c_w\right] \frac{dT}{dt} + \frac{d(\rho_v V_v)}{dt} (e_v - e_l) = \dot{Q} \tag{9}$$

For convenience, the difference in internal energies can be redefined in terms of the latent heat, pressure, and density by noting that:

$$L = e_v + \frac{p}{\rho_v} - e_l - \frac{p}{\rho_l} \tag{10}$$

Equation (9) can be rewritten as:

$$\left[\rho_v V_v c_v + \rho_l V_l c_l + \rho_w V_w c_w\right] \frac{dT}{dt} + \frac{d(\rho_v V_v)}{dt} \left[L - p\left(\frac{1}{\rho_v} - \frac{1}{\rho_l}\right)\right] = \dot{Q} \tag{11}$$

Expressing the derivatives in terms of pressure, the evolution equation for pressure becomes:

$$\frac{dp}{dt}\left\{\left[\rho_v V_v c_v + \rho_l V_l c_l + \rho_w V_w c_w\right] \frac{\partial T}{\partial p} + \frac{\partial(\rho_v V_v)}{\partial p} \left[L - p\left(\frac{1}{\rho_v} - \frac{1}{\rho_l}\right)\right]\right\} = \dot{Q} \tag{12}$$

The evolution equation for pressure is evolved in time using forward Euler time integration. $\frac{\partial T}{\partial p}$ is evaluated from the saturation curve specific to the fluid of interest. $\frac{\partial(\rho_v V_v)}{\partial p}$ is evaluated from the ideal gas law, saturation curve, and mass conservation equation. The mass conservation equation (Equation (3)) can be integrated in time to obtain:

$$V_v(\rho_v) = V_{v,o} \frac{\rho_l - \rho_{v,o}}{\rho_l - \rho_v} \tag{13}$$

where the subscript o denotes the initial vapor state. Expanding the derivative and invoking the ideal gas law for the vapor yields:

$$\frac{\partial(\rho_v V_v)}{\partial p} = \left(\rho_v \frac{\partial V_v}{\partial \rho_v} + V_v\right) \frac{\partial \rho_v}{\partial p} = \left(\rho_v \frac{\partial V_v}{\partial \rho_v} + V_v\right) \left(\frac{1}{RT} - \frac{p}{RT^2} \frac{\partial T}{\partial p}\right) \tag{14}$$

$\frac{\partial V_v}{\partial \rho_v}$ is computed analytically from Equation (13) and once again $\frac{\partial T}{\partial p}$ is evaluated from the saturation curve. The properties used to solve the pressure evolution equation, along with some system parameters, are given in Table 1.

IV. Results and Discussion

Before comparing the experimental results to the thermodynamic model, the effects of liquid fill fraction and heater power and distribution on the self-pressurization rate can be analyzed by studying the experimental data. The effect of heater power on the self-pressurization rate is shown in Figure 2. The specified heat powers are distributed evenly over the bottom heater for a 25% full tank. All curves show, after an initial transient, the tank pressure increases at a uniform rate. This is to be expected. The initial transience is driven by transport processes in the fluid, the formation of a natural convection boundary layer along the side wall and developing temperature gradients at the liquid-vapor interface. Once the initial transience subsides, the flow field and temperature field in the fluid are fully developed resulting in a stationary temperature field. While the temperature of the fluid will increase in time, the temperature gradients become time invariant – the temperature at any location in the fluid rises at the same rate. Since the pressurization rate is dependant on the difference in heat flux on the liquid and vapor sides of the interface, when the temperature

gradient becomes constant in time the tank pressure will increase at a uniform rate. The curves also reflect, quite intuitively, that the more heat is added to the system, the more rapidly tank pressure will increase. This behavior is consistant with the thermodynamic model derived earlier, since the heat entering the system acts as a source term on the right side of the pressure evolution equation (Equation (12)). Furthermore, the data shown in Figure 2b also reveal that the pressure response of the system is not immediate – the system pressure does not start increasing at time = 0 when heat begins to enter the system. It takes a finite amount of time for thermal energy entering the system from the heater to be carried, by convection currents, to the liquid-vapor interface. Once the thermal energy reaches the interface, evaporation can occur and the tank pressure will increase. At these early times, the tank pressure increases rapidly because of the large thermal gradients on the liquid side of the interface. However, once the flow field and temperature field in the liquid are well established, the temperature gradient becomes constant in time and the tank pressure will continue to increase at a constant rate but slower than the pressurization rate during the initial transient period.

The effect of fill fraction on tank pressure is shown in Figure 3. In all three cases presented in Figure 3, the heater in the liquid is supplying heat at a rate of 2 W. The data reveal that the initial pressure response lag increases with increasing fill fraction. This is due to the fact that at higher fill fractions, the axial distance between the interface and the heater increases. As a result, the time it takes the thermal energy to reach the interface also increases. The data in Figure 3 also reveals that the self-pressurization rate increases with increasing fill fraction. The effect on pressurization rate can be understood in terms of how energy entering the system is partitioned. When thermal energy enters the liquid from the heater, some of the energy is used to raise the temperature of the bulk liquid while some of the energy is used to evaporate liquid. When heat is being added to the liquid, the more liquid there is in the tank, the less thermal energy is available for evaporation. This decrease in the available energy for evaporation would be accompanied by a decrease in pressurization rate.

The effect of heating mode on tank pressurization is studied by varying the location of the heat input. The results are shown in Figure 4. Heat can be added directly to the liquid through the bottom heater, directly to the vapor through the top heater or to both phases through various combinations of the two heaters. In all the cases shown in the figure, the fill fraction is 50% and 2 W of heat enter the system. For the vapor-only and liquid-only heating cases, the 2 W is distributed evenly over the active heater. When both heaters are active, 1 W is distributed over each heater. Contrary to intuition, the liquid heating case results in the largest pressurization rate. Intuitively, one would expect that since energy is being directly added to the ullage for the vapor heating case, the pressurization rate should be greatest. This intuitive conclusion is also consistant with the liquid hydrogen experiments performed by Aydelott.[4] But unlike Aydelott's experiment, in the present experiment we are subject to severe wall effects. The wall effect arises because the thermal conductivity of the wall is more than an order of magnitude larger than the thermal conductivity of the vapor (see Table (1)). Since the heaters are mounted to the inside surface of the tank wall, when heat is applied to the heaters, much of the energy is going into the wall rather than into the ullage. This unfavorable mismatch in thermal conductivity would not be as severe a problem if, like Aydelott's experiment, the tank walls were sufficiently thin resulting in a negligible thermal inertia. In our experiment, the tank walls are not thin and thus the tank wall acts as a heat sink reducing the amount of heat actually going into the vapor. Since, for the vapor heating case, most of the thermal energy is going into the wall instead of being used to increase the internal energy of the vapor, the pressurization rate is the smallest. Furthermore, comparison between the three curves in Figure 4 suggests that the more heat is distributed over the heater located in the vapor, the smaller the self-pressurization rate will become.

While the thermal conductivity of the liquid is larger than that of the vapor, it is still smaller than the thermal conductivity of the wall. In all cases, therefore, part of the heat power distributed over the heaters goes into the tank wall. This is why it is necessary to include the thermal inertia of the tank wall in the thermodynamic model. The effect of the tank wall is clearly seen in Figure 5a. Here, we consider a 25% full tank subject to a liquid heating rate of 3 W. In this figure, the experimental data is compared to two different predictions of the thermodynamic model. In the first prediction, the upper curve in Figure 5a, the thermal inertia of the wall is neglected by removing the $\rho_w\, c_w\, V_w$ term in Equation (12). For the second prediction, the lower curve in Figure 5a, the effect of the wall is accounted for by retaining this term. Clearly, the presence of the wall has a drastic effect on the pressurization rate. When the wall effect is neglected, the pressurization rate is grossly overpredicted. In this case, the thermodynamic model implicitly assumes that the entire 3 W is going into the fluid. Since the wall is acting like a heat sink, the actual amount of heat entering the fluid is reduced, resulting in a smaller pressurization rate as indicated by the experimental

data. Taking into account the wall effect, by including the thermal inertia of the wall in the thermodynamic model, the predicted self-pressurization rate agrees well with the experimental data. For the vapor heating case, shown in Figure 5b, again the thermodynamic model without the wall effect drastically overpredicts the pressurization rate. Including the thermal inertia of the wall in the thermodynamic model reduces the deviation between the model's predictions and experimental results, but still, discrepancy exists. The source of this discrepancy will be discussed below.

Other representative comparisons between the thermodynamic model (including the effect of the wall) and the experimental results are shown Figure 6. In all the cases other then the vapor heating case, the thermodynamic model adequately predicts the pressurization rate, but does a poor job at predicting the actual value of tank pressure. The inability of the thermodynamic model to capture the initial pressure transience results in the discrepancy in the predicted value of tank pressure. Once the initial transience has subsided, the flow field and temperature field are fully developed and the temperature gradient becomes constant in time – the temperature at any location in the fluid rises at the same rate. Since this condition is the underlying assumption used to derive the *homogeneous* thermodynamic model, once the temperature field becomes stationary, the pressurization rates for both the thermodynamic model and the experiment will agree. When heat is added directly to the vapor, discrepancies between the model's predictions and the experimental results arise. The discrepancy is due to the unfavorable mismatch between thermal conductivies of the wall and vapor. The homogeneous thermodynamic model assumes that the incoming thermal energy is evenly distributed between the liquid, vapor, and tank wall. Since for the vapor heating mode, the incoming energy is almost all going into the wall, deviation between the thermodynamic model and the experimental results is expected. Even though there is an unfavorable mismatch between the thermal conductivities of the wall and liquid, the deviation due to this mismatch is not noticeable. The reasons for this are twofold. First, while less than the thermal conductivity of the wall, the conductivity of the liquid is still significantly larger than that of the vapor. Thus for liquid heating mode, even though some heat is lost to the wall, more heat would enter the liquid/vapor system. Secondly, and more importantly, because of buoyancy, any heat entering the liquid through the side wall would lead to convective mixing of the thermal energy in the liquid. Since the thermodynamic model implies that the energy in the liquid phase is distributed homogeneously, any convective mixing in the liquid would increase the degree of homogeneity yielding a better agreement with the model's predictions.

Another shortcoming of the thermodynamic model is that the effect of heat distribution on tank self-pressurization is not taken into account. This is clearly shown in Figure 6c. Although counterintuitive, the experimental data in this figure clearly show that the manner in which heat is distributed on the side wall has a definate effect on the pressurization rate. The effect is not accounted for by the thermodynamic model, since application of the model to the three cases in Figure 6c yields the identical result. As far as the model is concerned, for all three cases, 2 W of heat is entering the system. Based on that heat input, the model predicts the same pressurization rate for the three cases. There is no mechanism in the thermodynamic model account for how those 2 W are distributed along the tank wall.

V. Conclusions

The effects of heat power and distribution and fill fraction on the self-pressurization of a model fluid experiment in normal gravity was investigated. In all the cases considered, a lag in the pressure response of the system was observed. The lag in response increased with increasing liquid fill fraction. This lag was due to the finite amount of time it took thermal energy to be carried from the heater to the liquid-vapor interface. Once this thermal energy reached the interface, evaporation occurred resulting in tank self-pressurization. In these early stages of the pressurization process, developing temperature gradients in fluid caused the system to undergo an initial transience. Once these initial transients subsided, any thermal gradients in the fluid became time invariant resulting in a uniform pressurization rate.

Furthermore, results indicated an increase in heater power and a decrease in fill fraction both led to an increase in pressurization rate. Results also showed that applying the heat to the liquid led to a greater pressure rise than applying the heat directly to the vapor. This unexpected result was obtained because the low thermal conductivity of the vapor resulted in most of the heat going direclty into the tank wall rather than into the ullage. To investigate this effect further, a homogeneous thermodynamic model was developed that included the thermal inertia of the tank wall. For all the liquid heating cases, comparsions showed excellent agreement between the predicted and measured pressurization rate. However, the inability of the

thermodynamic model to capture the initial pressure behavior led to a discrepancy in the magnitude of the tank pressure between the model's predictions and the experimental results. For the vapor heating case, the predicted pressurization rate did not agree with the experimental data. This deviation was primarily due to the unfavorable mismatch between the thermal conductivites of the wall and vapor. Resolving the shortcomings in the thermodynamic model by developing of a comprehensive two-phase CFD model for tank pressurization will be the subject of future work.

References

[1]Clark, J. A., *A Review of Pressurization, Stratification, and Interfacial Phenomena*, Int. Advances in Cryogenic Engineering, Plenum Press, 1965, pp. 259–283.

[2]Aydelott, J. C., Carney, M. J., and Hochstein, J. I., "NASA Lewis Research Center Low-Gravity Fluid Management Technology Program," NASA TM 87145, 1985.

[3]Plachta, D. W. and Kittel, P., "An Updated Zero Boil-Off Cryogenic Propellant Storage Analysis Applied to Upper Stages or Depots in an LEO Environment," AIAA 2002-3589, 2002.

[4]Aydelott, J. C., "Effect of Gravity on Self-Pressurization of Spherical Liquid Hydrogen Tankage," NASA TN D-4286, 1967.

[5]Liebenberg, D. H. and Edeskuty, F. J., *Pressurization Analysis of a Large-Scale Liquid Hydrogen Dewar*, Int. Advances in Cryogenic Engineering, Plenum Press, 1965, pp. 284–289.

[6]Aydelott, J. C. and Spuckler, C. M., "Effect of Size on Normal-Gravity Self-Pressurization," NASA TN D-5196, 1969.

[7]Riemer, D. H., *Cryogenic Tank Stratification: A Simpler Approach*, Vol. 31 of *Advances in Cryogenic Engineering*, Plenum Press, 1986, pp. 957–962.

[8]Lin, C. S., VanDresar, N. T., and Hasan, M. M., "Pressure Control Analysis of Cryogenic Storage Systems," *J. Propulsion and Power*, Vol. 20, No. 3, 2004, pp. 480–485.

[9]Arnett, R. W. and Voth, R. O., "A Computer Program for the Calculation of Thermal Stratification and Self-Pressurization in a Liquid Hydrogen Tank," NASA CR 2026, 1972.

[10]Tatom, J. W., Brown, W. H., Knight, L. H., and Coxe, E. F., *Analysis of Thermal Stratification of Liquid Hydrogen in Rocket Propellant Tanks*, Vol. 9 of *Advances in Cryogenic Engineering*, Plenum Press, 1964, pp. 265–272.

[11]Tanyun, Z., Zhongping, H., and Li, S., *Numerical Simulation of Thermal Stratification in Liquid Hydrogen*, Vol. 41 of *Advances in Cryogenic Engineering*, Plenum Press, 1996, pp. 155–161.

[12]Lin, C. S. and Hasan, M. M., "Numerical Investigation of the Thermal Stratification in Cryogenic Tanks Subjected to Wall Heat Flux," NASA TM 103194, 1990.

[13]Grayson, G. D., "Coupled Thermodynamic-Fluid-Dynamic Solution for a Liquid Hydrogen Tank," *J. Spacecraft and Rockets*, Vol. 32, No. 5, 1995, pp. 918–921.

[14]Panzarella, C. H. and Kassemi, M., "On the Validity of Purely Thermodynamic Descriptions of Two Phase Cryogenic Fluid Storage," *J. Fluid Mech.*, Vol. 484, 2003, pp. 41–68.

Table 1. Thermophysical Properties and Representative System Parameters

Parameter	Value	Parameter	Value	Parameter	Value
ρ_l	1400 kg/m^3	ρ_v	5.56 kg/m^3	ρ_w	1190 kg/m^3
c_l	1300 J/kg K	c_v	730 J/kg K	c_w	1500 J/kg K
k_l	0.075 W/m K	k_v	0.01 W/m K	k_w	0.2 W/m K
L	142000 J/kg	V_w	0.00741 m^3	V_T	0.01402 m^3
R	41.5725 J/kg K	T	298 K	p	64600 Pa

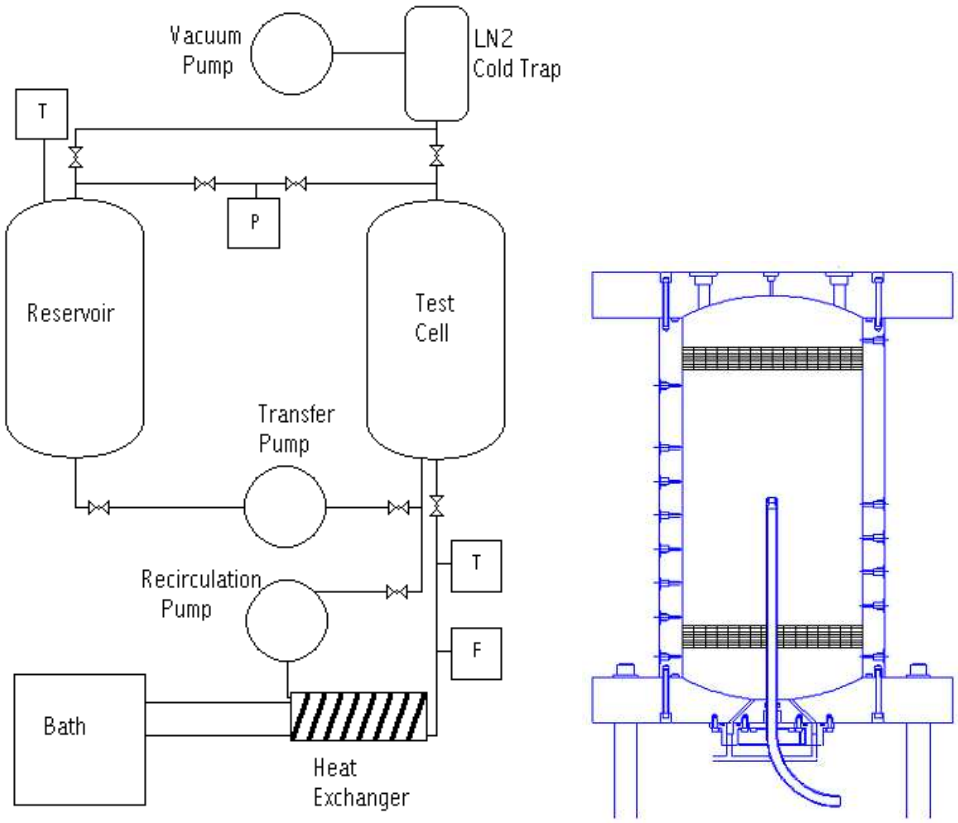

(a) (b)

Figure 1. Experimental apparatus (a) with detailed view of the test cell (b)

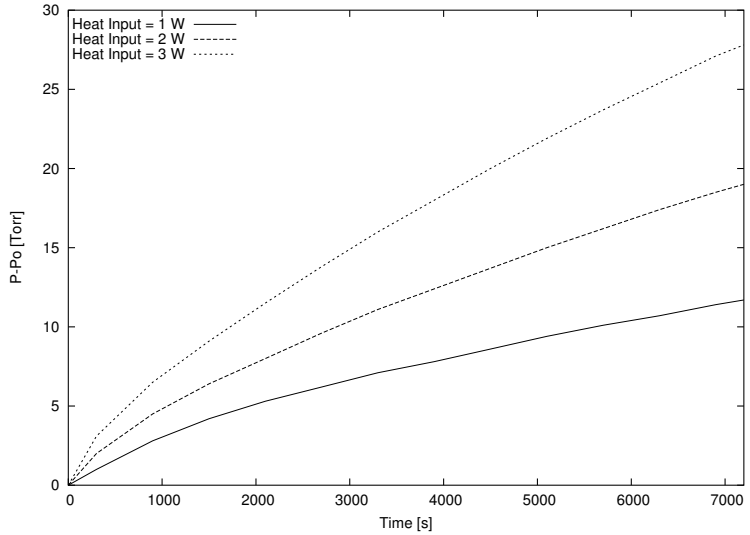

(a)

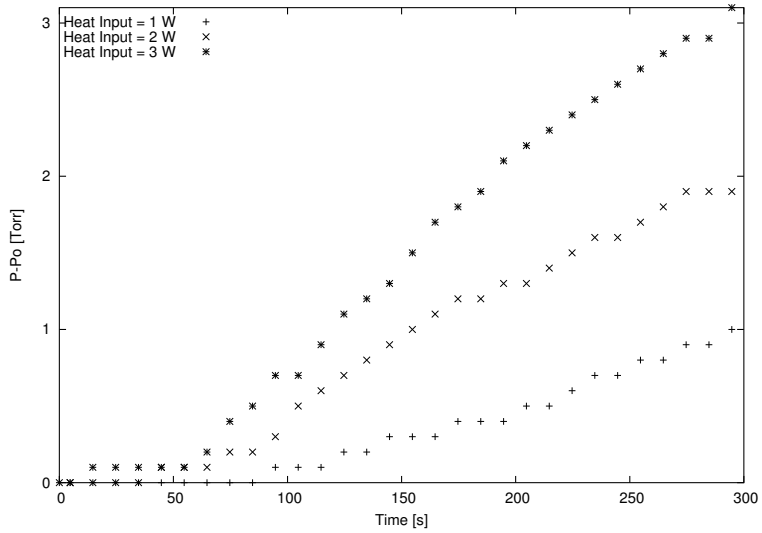

(b)

Figure 2. Effect of heat power on tank pressure (Fill Fraction = 25%, Liquid Heating)

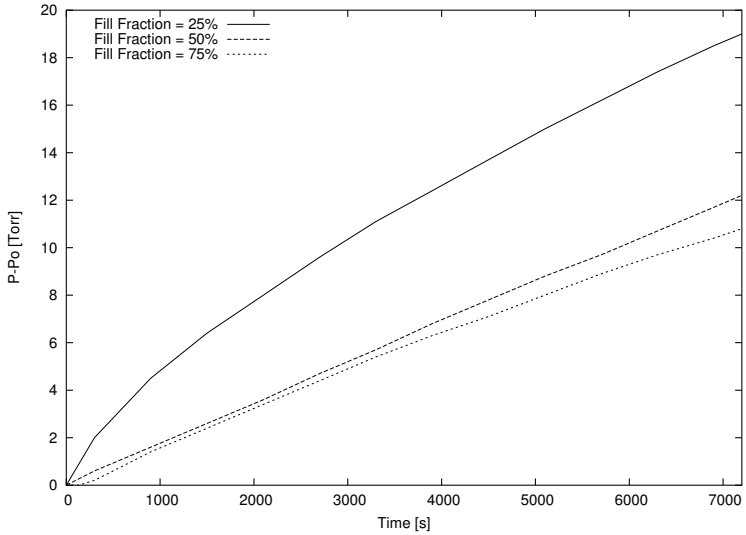

(a)

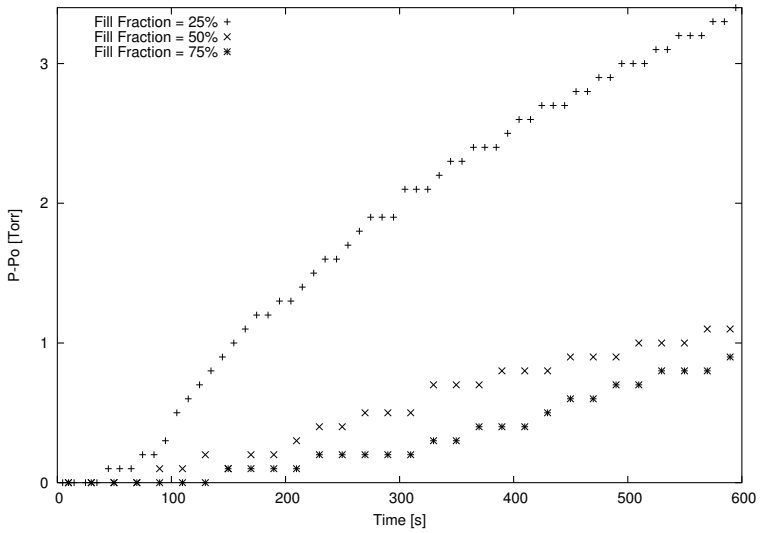

(b)

Figure 3. Effect of fill fraction on tank pressure (Heat Input = 2 W, Liquid Heating)

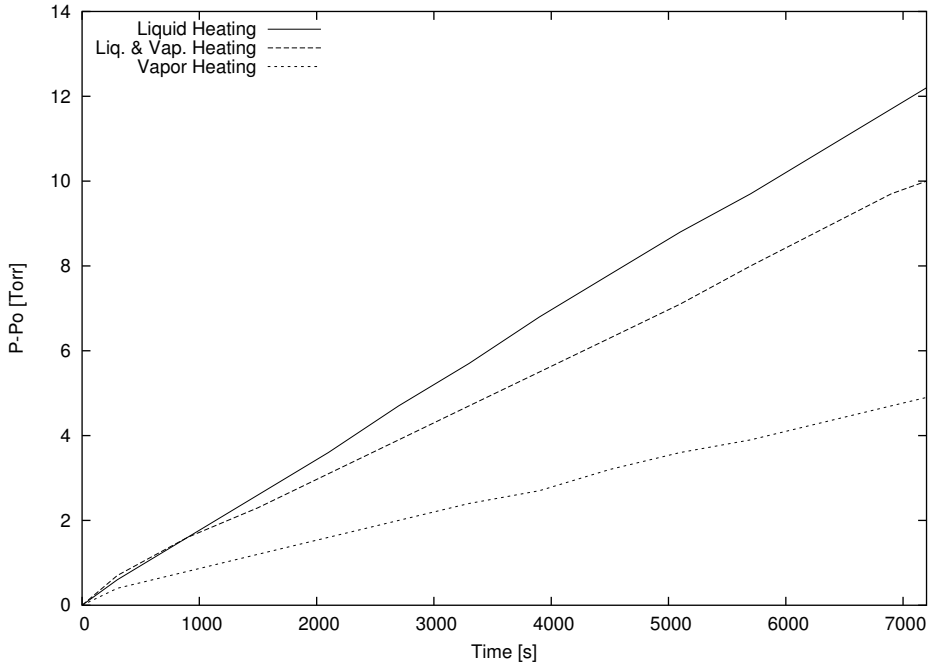

Figure 4. Effect of heat distribution on tank pressure (Fill Fraction = 50%, Heat Input = 2 W)

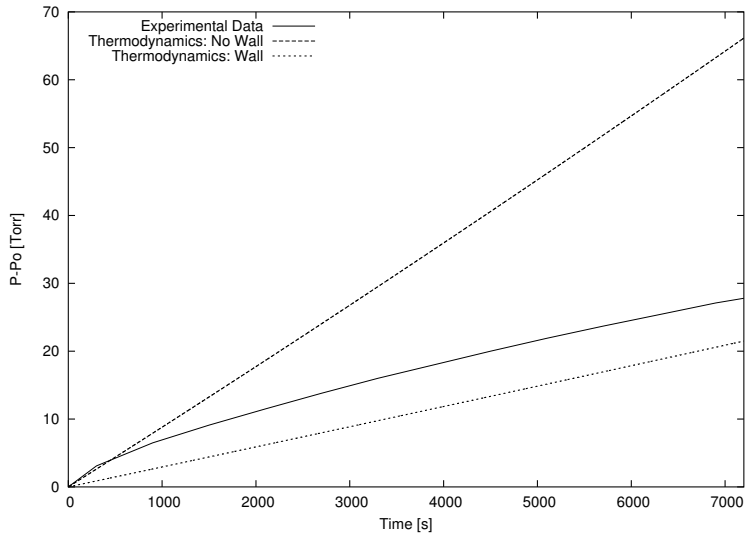

(a) Fill Fraction = 25%, Heat Input = 3 W, Liquid Heating Heating

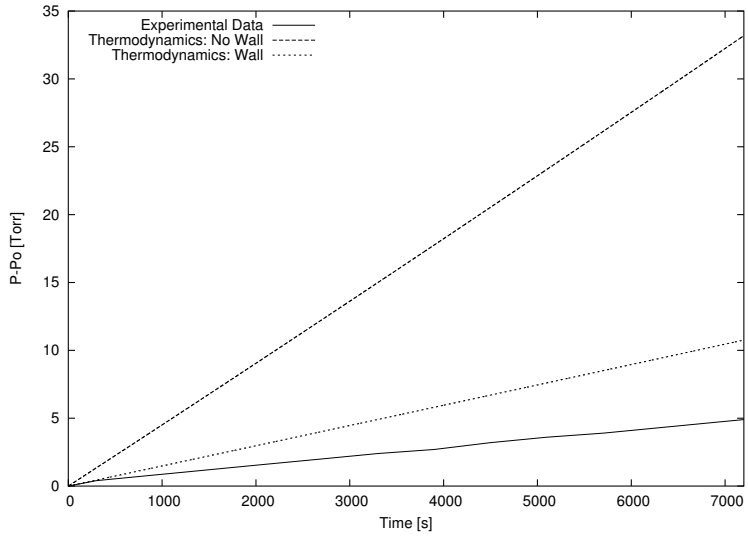

(b) Fill Fraction = 50%, Heat Input = 2 W, Vapor Heating

Figure 5. Comparisons between the experimental data and the thermodynamic model both with and without the effects of the tank wall.

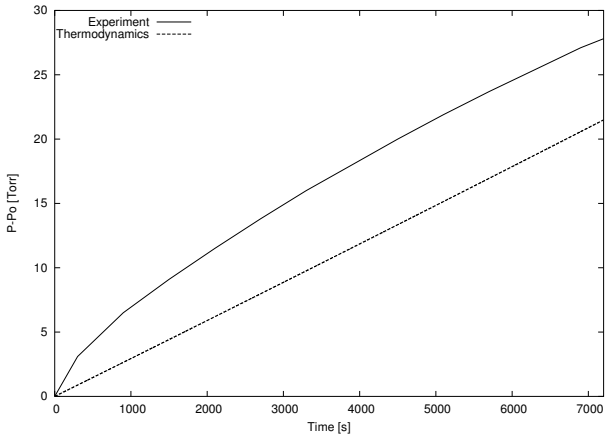

(a) 25% Full, Bottom Heating, Heat Input = 3 W

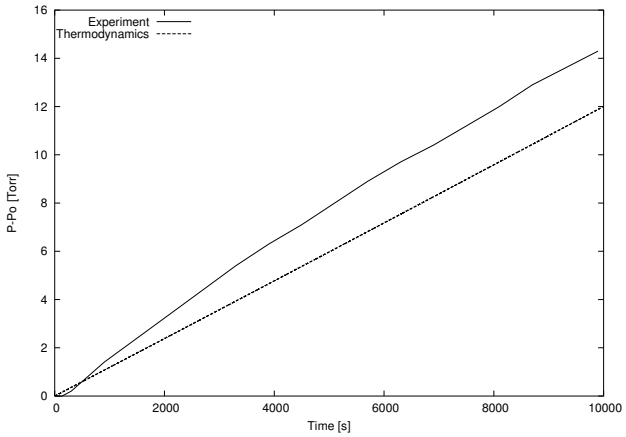

(b) 75% Full, Bottom Heating, Heat Input = 2 W

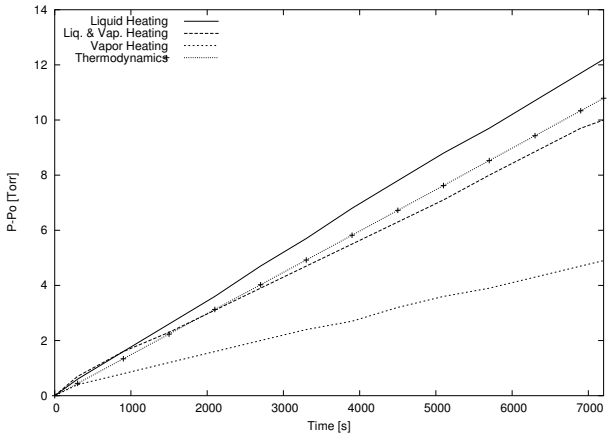

(c) 50% Full, Heat Input = 2 W

Figure 6. Representative comparisons between the experimental results and thermodynamic model.